Phys. Status Solidi B **249**, No. 5, 900–906 (2012) / **DOI** 10.1002/pssb.201100085

physica status solidi b
www.pss-b.com
basic solid state physics

Feature Article

Excitonic signatures in the optical response of single-wall carbon nanotubes

Christophe Voisin[*,1], Sébastien Berger[1], Stéphane Berciaud[2], Hugen Yan[3,†], Jean-Sébastien Lauret[4], Guillaume Cassabois[1,‡], Philippe Roussignol[1], James Hone[3], and Tony F. Heinz[3]

[1] Laboratoire Pierre Aigrain, École Normale Supérieure, CNRS UMR8551, UPMC, Université Paris Diderot, 24 rue Lhomond, 75005 Paris, France
[2] IPCMS, UMR 7504, CNRS Université de Strasbourg, 23 rue du Loess, 67034 Strasbourg, France
[3] Physics, Mechanical Engineering and Electrical Engineering Departments, Columbia University, New York, NY, USA
[4] Laboratoire de Photonique Quantique et Moléculaire, École Normale Supérieure de Cachan, CNRS UMR 8537, Institut Dalembert, 61 Avenue Wilson, Cachan, France

Received 29 April 2011, revised 13 December 2011, accepted 14 December 2011
Published online 30 January 2012

Keywords carbon nanotubes, excitons, photoluminescence, Rayleigh scattering

[*] Corresponding author: e-mail christophe.voisin@lpa.ens.fr, Phone: +33 1 44 32 38 45, Fax: +33 1 44 32 38 40
[†] Present address: IBM T.J. Watson Research Center, Yorktown Heights, NY, USA
[‡] Present address: Laboratoire Charles Coulomb, Université de Montpellier, Montpellier, France

The optical properties of single-wall carbon nanotubes (SWNTs) are dominated by the excitonic character of the transitions even at room temperature. The very peculiar properties of these excitons arise from both the one-dimensional (1D) nature of carbon nanotubes and from the electronic properties of graphene from which nanotubes are made. We first propose a brief qualitative review of the structure of the excitonic manifold and emphasize the role of dark states. We describe recent experimental investigations of this excitonic structure by means of temperature dependent PL measurements. We investigate the case of upper sub-bands and show that high-order optical transitions remain excitonic for large diameter nanotubes. A careful investigation of Rayleigh scattering spectra at the single nanotube level reveals clear exciton–phonon side-bands and Lorentzian line profiles for all semi-conducting nanotubes. In contrast, metallic nanotubes show an ambivalent behavior which is related to the reduced excitonic binding energy.

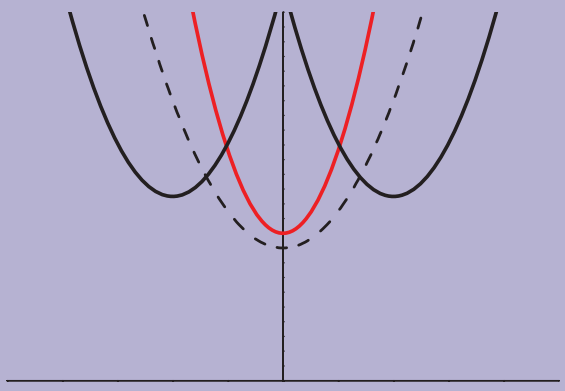

Schematic of the exciton manifold in single-wall carbon nanotubes.

1 Introduction Single-wall carbon nanotubes (SWNTs) consist of a single rolled-up graphene sheet with a typical diameter in the nanometer range and a typical length of the order of one micrometer. Most of their peculiar properties arise from their quasi one-dimensional (1D) character with aspect ratios that usually reach 10^3. These nanotubes are envisioned for a number of applications ranging from mechanical reinforcement, medical applications [1], nonlinear optics [2], or opto-electronic devices [3]. In particular, their opto-electronic properties are dominated by the strong Coulomb interactions typical of 1D properties: optical excitations lead to the formation of strongly bound electron–hole pairs known as excitons, with binding energies of the order of a few hundreds of meV. Therefore, even for room temperature applications, it is essential to have the best possible understanding of these excitonic properties. In this paper, we will review the recent advances in the description and in the experimental

investigation of excitons in carbon nanotubes. We will show that advanced spectroscopic studies allow to access most of the states of the excitonic manifold and provide a detailed and quantitative picture of the excitonic fine structure.

2 Theoretical approach The geometry of a nanotube is entirely determined by two integer numbers n and m thereafter called the chiral indices that represent the coordinates of the circumference vector in the graphene lattice basis [4].

2.1 The zone-folding method In a first approximation, the electronic and optical properties of SWNTs can be deduced from those of graphene simply by considering the quantization of the wave vector in the circumference direction, a method which is known as the zone-folding method. Due to the symmetry of the graphene band structure with respect to the Fermi level, this description leads to a set of symmetrical quasi-hyperbolic 1D sub-bands in the valence and conduction bands. Important corrections to this picture appear when taking into account the warping of the graphene bands due to the trigonal symmetry [5]. Each sub-band is fourfold degenerate (two times for the K, K' valley degeneracy and two times for the spin). Each sub-band gives rise to a so-called van Hove singularity in the density of states. In addition, for metallic nanotubes, defined by $n - m = 0 \bmod 3$, two additional linear bands crossing at the Fermi level give rise to a non-vanishing density of states at the Fermi level. For dipolar optical transitions with an electrical field polarized along the tube axis, selection rules apply that only allow transitions between two symmetrical sub-bands [6]. These transitions are referred to as $S_{11}, S_{22}, \ldots, S_{ii}$ transitions for semi-conducting nanotubes and M_{ii} transitions for metallic nanotubes (cf. Fig. 1).

2.2 Excitons When Coulomb interaction between carriers is taken into account, the electron and the hole created in an optical transition are taken to a bound state and the band-gap is renormalized. Both effects are of considerable magnitude (on the order of the band-gap itself for semi-conducting nanotubes), but almost cancel each other. In total, the energy of the transition is relatively close to the one expected from the zone-folding method whereas the nature of the excitation is completely different. Each excitonic state is in principle 16 times degenerate, with 12 triplet states and 4 singlet states. Only the latter are accessible in dipolar optical transitions. However, the electron–hole interaction lifts the fourfold degeneracy of the singlet states, leading to the excitonic scheme depicted in Fig. 2 [7, 8]. Two bands that are formed with an electron and a hole from the same valley, have their energy minimum for vanishing center of mass momentum. The zone-center wave function of the lowest band is symmetric in the coordinate along the tube axis, whereas the upper one is anti-symmetric. The two-other bands hereafter referred to as KK' excitons, arise from an electron and a hole taken from each valley. Therefore their energy minimum occurs for non-vanishing center of mass

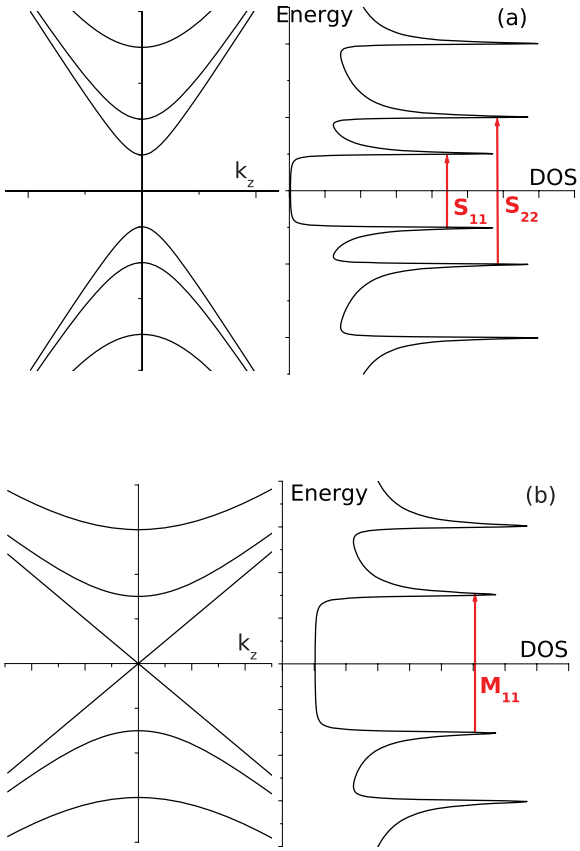

Figure 1 (online color at: www.pss-b.com) Schematic band structure and related density of states of (a) a zig-zag semi-conducting (b) a metallic nanotube in the conical approximation. Arrows indicate allowed dipolar optical transition for a polarization along the nanotube axis.

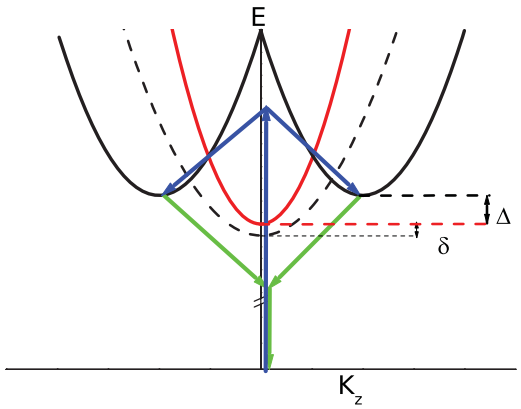

Figure 2 (online color at: www.pss-b.com) The four singlet excitonic states in a chiral nanotube resulting from the mixing of two pairs of electrons and holes states from the K and K' valleys. The red line corresponds to the bright state. The solid black lines correspond to the so-called KK' excitons. The dashed line is the dark exciton of even symmetry. The blue arrows depict the indirect absorption process leading to a phonon side-band, whereas the green arrows depict the reciprocal emission process.

wave vector and their pseudo-angular momentum is in general not 0. Therefore, these excitonic branches cannot directly couple to light. Within a given sub-band, this excitonic scheme is repeated for each hydrogenic level of the electron–hole pair, labeled by the principal quantum number n. In 1D, this quantum number also sets the parity of the envelope function which is opposite to that of the quantum number itself. Therefore, among the two lowest excitonic states, only one has the global odd parity (u) required for dipolar optical transitions. For the lowest transition ($n=1$), the lower zone-center excitonic state is dark (hereafter labeled $1g$) whereas the upper one is bright ($1u$). We will see in the following the important consequences of this point on the optical properties of carbon nanotubes. For the next hydrogenic state ($n=2$), the situation is inverted (see Fig. 5).

3 Excitonic fine structure of the S_{11} sub-band

3.1 Seeking for the dark state As explained in Section 2.2, the lowest state of the S_{11} excitonic manifold is expected to be dipole forbidden, which may have drastic consequences on the photoluminescence (PL) properties of nanotubes if the energy splitting with the bright state is significant. A natural way to address this point is perform temperature dependent PL measurements. This requires to have solid-state light emitting samples of carbon nanotubes. This point is not straight forward since powders of carbon nanotubes are known to show efficient quenching of PL [9, 10] due to tube–tube interactions in bundles and especially quenching of semi-conducting nanotubes by neighboring metallic nanotubes. The regular method to circumvent this effect, is to disperse the nanotubes in water suspensions by means of a surfactant that prevents re-bundling of the nanotubes [11]. We further incorporate gelatin to this suspension [12] in order to obtain a solid state film that preserves the micelle structure as evidenced by the equivalent PL level compared to the initial suspension. This solid state film may be cooled down to cryogenic temperatures and heated back to room temperature for several cycles without any apparent change in the optical properties.

The data in Fig. 3 shows the evolution of the PL intensity of (9,4) semi-conducting nanotubes as a function of the temperature. The PL intensity shows a maximum at about 40 K. The PL intensity decreases for higher temperatures, which is the regular behavior in semi-conductors, usually attributed to the activation of non-radiative recombination channels. More intriguing is the sudden drop of the PL intensity at lower temperatures (between 40 and 10 K). This unusual behavior is interpreted as a consequence of the trapping of excitons on the dark state at low temperature. This temperature profile can be accounted for by means of a simplified three-level model, as depicted in the inset of Fig. 3. The upper state (B) stands for the zone-center bright excitonic state whereas (D) stands for the dark state and (G) for the ground state. (D) and (B) are supposed to be coupled in a efficient enough way so to reach thermal equilibrium of

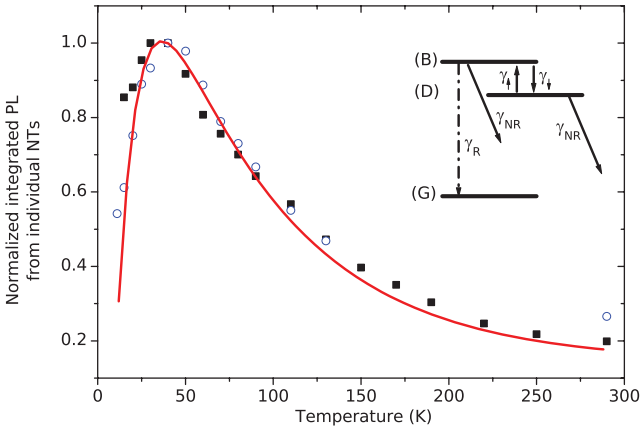

Figure 3 (online color at: www.pss-b.com) Integrated photoluminescence intensity of (9,4) nanotubes embedded in a gelatin matrix as a function of the temperature. The black squares and the open circles correspond to two sets of data obtained in different experimental setups. The red solid line is a fit to the data using a three level scheme as depicted in the inset. The dark/bright state splitting deduced from the fitting is 3 meV $\pm$ 0.5.

their populations. (Note however that other groups used a non-thermal distribution among these sates to account for bi-exponential decays [13, 14].) Both (B) and (D) states are non-radiatively coupled to the ground state with a rate γ_{NR} taken equal for both states for the sake of simplicity. Finally (B) is coupled to the ground state through a radiative rate γ_R. The values for γ_{NR} were extracted from previous time-resolved PL measurements [12] and γ_R reads $\gamma_R \propto \gamma_0/\sqrt{T}$ for a 1D system. The agreement with experimental data is excellent and allows to extract the energy splitting between the dark and bright state for (9,4) nanotubes. It turns out to be $\delta = 3 \pm 0.5$ meV. This relatively small value (compared to theoretical predictions in the range of a few tens of meV [15, 16]) means that the dark and bright states are almost equally populated at room temperature. Therefore, the existence of this dark state cannot in itself explain the very weak PL quantum yields reported for carbon nanotubes. In this context, the role of triplet states that are predicted to lie far below the singlet states [15] remains to be explored.

This procedure can be repeated for other chiral species by means of selective PL. The values of the dark/bright state splitting as a function of the nanotube diameter are reported in Fig. 4. This splitting is clearly a decreasing function of the tube diameter. However, the precision of the measurements does not allow to distinguish between possible $1/d$ and $1/d^2$ laws [17].

Another approach has been reported to probe the existence of this dark state by applying a magnetic-field along the tube axis. This kind of measurement was made either in ensembles of nanotubes [18] or at the individual nanotube level [19, 20]. This magnetic field brakes the K–K' symmetry and induces a partial brightening of the lowest state. By measuring PL spectra as a function of the applied field, it is possible to extrapolate the value of the dark/bright state splitting at zero field. This estimated

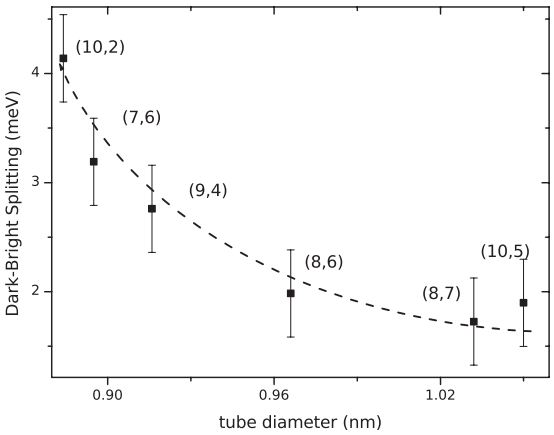

Figure 4 Dark/bright state splitting δ *versus* the diameter of the nanotube. The dashed line is a guide to the eyes.

splitting turns out to be exactly in the same range of energies as the one deduced from temperature dependent PL measurements (as discussed above) confirming the interpretation in terms of intrinsic effects.

3.2 Two-photon absorption and even excitonic states The existence of excitonic states with even symmetry can be probed by means of two-photon spectroscopy. Although the lowest dark state could in principle be seen in two-photon absorption, its splitting with the bright state is too weak to allow unambiguous identification. In contrast, the even state corresponding to $n=2$ (second hydrogenic level) and usually denoted $2g$ [21] can be excited by means of two-photon absorption. After subsequent non-radiative relaxation to the $1u$ state, this will give rise to luminescence. This so-called two-photon excitation of luminescence is actually the method that was used independently by two groups for proving the existence of excitons in carbon nanotubes [21, 22]. The splitting between the PL photon energy and twice the excitation photon energy (i.e., the $2g-1u$ splitting) allows to estimate the exciton binding energy from an extrapolation of the Rydberg series.

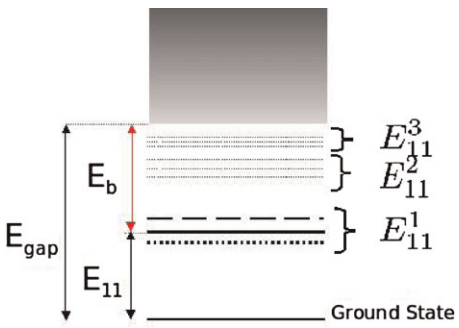

Figure 5 (online color at: www.pss-b.com) Schematic of the Rydberg series of excitons in SWNTs. The superscript stands for the Rydberg principal quantum number. For each value of the latter four singlet states exist, two of them being degenerate and one of them only being bright.

3.3 *KK′* excitons As explained in Section 2.2, two of the four states of each hydrogenic level are formed from an electron and a hole belonging to different valleys, leading to excitonic states with in general non-vanishing quasi angular momentum and having their energy minimum off the center of the Brillouin zone. These states cannot couple directly to light. However, an indirect process involving the emission of an optical phonon carrying the required momentum and angular momentum is still possible [23]. These indirect processes are depicted in Fig. 2 with blue arrows for the absorption process and green arrows for the emission process. They lead to phonon-side bands in absorption and PL spectroscopy. Such side-bands have been first reported by several teams [24–27]. The key point is that these side-bands are not symmetrical (in energy) with respect to the bright state but rather with respect to the KK' dark ones (which are degenerate in energy). Therefore, measuring both the absorption and emission side-bands of a given chiral species allows the determination of the KK' exciton energy and that of the phonon mode involved in the process. This measurement has been performed by several teams [28, 29]. It turns out that the energy splitting between the bright and the KK' exciton is on the order of 35 meV, with a weak dependence on the diameter and chiral angle showing however characteristic family patterns [29]. The phonon mode is a close to zone-edge optical phonon with a typical energy of 165 meV.

3.4 Upper hydrogenic levels Apart from two-photon absorption that allowed the observation of even states of the second hydrogenic level (see Section 3.2), additional odd states of higher hydrogenic levels can be accessed by linear excitation of PL (Fig. 5). Experiments conducted on single suspended nanotubes by Lefebvre and Finnie [30] unambiguously showed three hydrogenic levels ($1u$, $2u$, and $3u$) with decreasing oscillator strength, together with the threshold of the continuum of band to band transitions.

4 Excitons of upper sub-bands While the excitonic structure of S_{11} transitions – and to some extend that of S_{22} – has been largely discussed in the literature, the nature of the transitions between upper sub-bands (namely S_{33}, S_{44}) remains unclear. One could qualitatively argue that due to the overlap between possible S_{33} excitons and the continuum of the lower sub-bands, such excitons should dissociate and that optical transitions should rather occur between free electron–hole pairs (regular band to band transitions). Furthermore, recent investigations of these sub-bands by resonant Raman spectroscopy showed that their energies do not follow the scaling law (transition energy corrected from the trigonal warping effect as a function of a reduced diameter) observed for S_{11} and S_{22} transitions [31, 32] and predicted theoretically [33]. Understanding the nature of

these upper transitions is of particular importance for applications since for nanotubes of diameter in the range of 2–3 nm, as usually obtained in regular growth conditions, these transitions lie in the visible part of the spectrum. Therefore, they may be the ones involved in opto-electronic applications of carbon nanotubes. Investigation of these upper transitions at the single nanotube level is limited to a small range of experimental techniques. In fact, due to the coupling with lower sub-bands these transitions show almost no luminescence. In addition, neither can they be accessed by excitation of luminescence spectroscopy since the S_{11} transitions for such diameters lie in the mid-infrared region where no low noise detectors are available.

4.1 Rayleigh scattering spectroscopy We proposed a new approach based on Rayleigh scattering spectroscopy of individual suspended nanotubes to address the question of the nature of high-order transitions in carbon nanotubes [34]. The details of the technique were published elsewhere [35]. In brief, carbon nanotubes are grown across 50 μm wide slits and excited with a broad spectrum light beam. The scattered light is collected in a 90° configuration and dispersed by a spectrometer. The spectra are corrected from the source spectrum and the regular $1/\lambda^3$ dependence of Rayleigh scattering for 1D systems. Due to the d^4 dependence of the scattered intensity, small bundles are easily distinguished from truly individual nanotubes. For the latter, each electronic resonance leads to enhanced Rayleigh scattering intensity that scales like $|\chi(\omega)|^2$, where $\chi(\omega)$ stands for the dielectric susceptibility. From previous studies [5] combining Rayleigh and Raman spectroscopies together with TEM diffraction measurements, it is possible to assign each Rayleigh spectrum to a specific chiral species. The diameter of the nanotube and its type (semi-conducting or metallic) are further confirmed in Raman spectroscopy by the RBM frequency and the bi-modal shape of the G-mode, respectively (see inset of Fig. 6).

4.1.1 Semi-conducting nanotubes The use of an improved super-continuum source led to unprecedented signal to noise ratio that allowed us to resolve fine structures in the spectra and perform reliable line-shape analysis. As shown in Fig. 6, we observed systematically pronounced side-bands ca 200 meV above each main electronic transition (i.e., S_{33}, S_{44}, and even S_{55} for the largest nanotubes). These distinct features are similar to the side-bands observed in absorption or PLE of lower transitions and correspond to the phonon mediated absorption of the dark KK' exciton. The observation of clear side-bands for S_{33} and S_{44} is a strong indication of the excitonic nature of upper transitions. From the value of the zone-edge optical phonon (as measured from the D band Raman line), we deduce that the splitting between this KK' exciton and the bright exciton is also on the order of 35 meV for upper sub-bands. This value, very similar to the one reported for S_{11} and S_{22} [24, 28], is quite surprising since this splitting was expected to depend on the diameter and the transition order. We attribute the coincidence to an

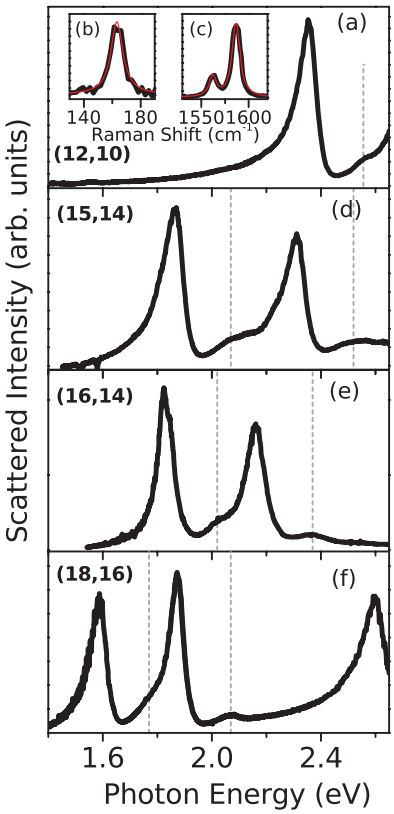

Figure 6 (online color at: www.pss-b.com) Rayleigh scattering spectra of several individual suspended nanotubes (a), (d), (e), and (f). The nature and diameter of the tube are further confirmed by Raman scattering as indicated for the first tube in the inset (b) for the RBM mode and (c) for the shape of the G mode. The phonon side-bands are visible ca. 200 meV above each resonance as indicated by the gray vertical lines.

accidental compensation of the scalings with the diameter and the local dielectric constant.

In order to go further in the determination of the excitonic nature of these upper transitions, we performed a careful line-shape analysis of the main excitonic lines. We compared the experimental profiles against an excitonic model (Lorentzian complex susceptibility $\chi(\omega) \propto 1/((\omega - \omega_0) - i\gamma/2))$ and a band-to-band transition model. In the case of 1D quasi-parabolic bands and neglecting the k dependence of the matrix element, we computed numerically the real and imaginary parts of the susceptibility. In total, the experimental spectra are fitted to $|\chi(\omega) + \chi_b|^2$ where χ_b stands for a real, spectrally flat background component arising from non-resonant transitions or from contributions of the environment. As shown in Fig. 7, the excitonic model is best suited to reproduce the experimental data: the band-to-band model always overestimates the blue side of the resonance, which reflects the asymmetric shape of van Hove singularities in the density of states.

This line-shape analysis, together with the systematic observation of phonon side-bands strongly suggests that

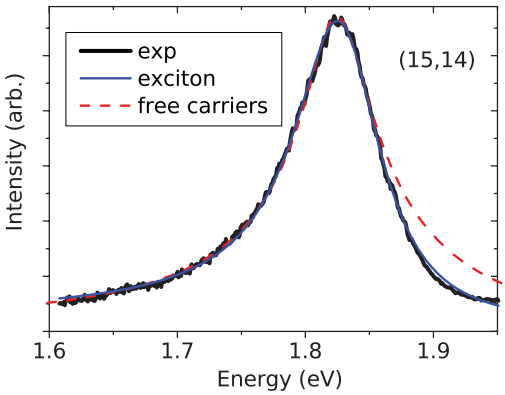

Figure 7 (online color at: www.pss-b.com) Rayleigh scattering spectrum of a single (15,14) semi-conducting nanotube. The scattering profile is fitted to either an excitonic model (Lorentzian susceptibility, blue solid line) or a band-to-band model (red dashed line).

upper transitions remain excitonic in nature. However, the coupling to lower continua shows up in the line-width of the transitions that can reach up to 80 meV. This corresponds to a dephasing time on the order of a few femtoseconds. This is consistent with the upper bound set by the very fast relaxation times observed in time-resolved spectroscopy for upper transitions [9, 36]. However, this line-width remains almost one order of magnitude smaller than the binding energy of such excitons, which probably explains the observation of bound states.

4.1.2 Metallic nanotubes The question of excitonic excitations in metallic materials is very peculiar in 1D systems since the reduced screening of Coulomb interactions can lead to bound electron–hole pairs even in the presence of free carriers [37–39]. This has been observed experimentally

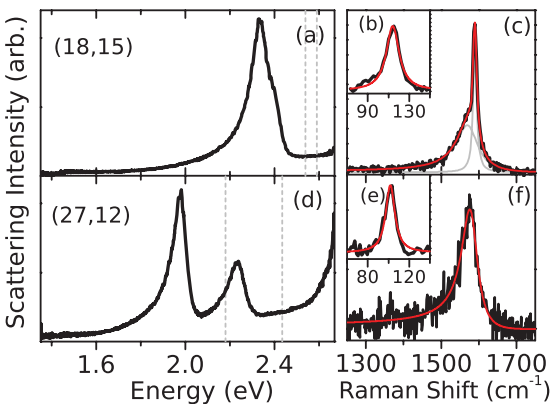

Figure 8 (online color at: www.pss-b.com) Rayleigh scattering spectra of two individual metallic nanotubes (a) and (d). The chiral indices are indicated. The diameter and the nature of the tube are further confirmed by Raman scattering as shown in the right column for the RBM mode (b) and (e) and the G mode (c) and (f). The gray vertical lines indicate the place where phonon side-bands could be expected.

in the case of metallic nanotubes by means of absorption spectroscopy [40] and Raman spectroscopy [41] for the lowest inter-sub-band transition M_{11}. The excitonic binding energy, however, turned out to be one order of magnitude weaker than in semi-conducting nanotubes. The Rayleigh scattering technique described in Section 4.1.1 allowed us to address this question for M_{22} transitions. The Rayleigh scattering spectra of several metallic nanotubes is displayed in Fig. 8 showing the typical splitting due to trigonal warping [5]. No sizable side-bands are observed for M_{22} transitions. This strongly contrasts with the case of semi-conducting nanotubes. However, the line-shape analysis still shows a better match with a Lorentzian shape rather than with a band-to-band model. We interpret this ambivalent signature as a consequence of the much reduced exciton binding energy in the case of metallic nanotubes.

5 Conclusion We have shown that the excitonic fine structure in SWCNTs is now well understood theoretically and supported by consistent experimental investigations. In particular, all the singlet states can be probed by optical spectroscopy: either magneto-spectroscopy or temperature dependent PL spectroscopy for zone-center excitons, or side-band spectroscopy for KK' excitons. The upper hydrogenic levels of the excitons series were accessed by means of either nonlinear spectroscopy for the even states or linear PLE for the odd states. Rayleigh spectroscopy also allowed to bring evidence for the excitonic nature of high-order transitions (S_{nn}) in large diameter semi-conducting nanotubes. Regarding metallic nanotubes, linear absorption spectroscopy also allowed to prove the existence of bound electron–hole pairs for the lowest transition. The case of high-order transitions in metallic nanotubes is more ambiguous, with transitions exhibiting Lorentzian line-shapes without clearly detectable side-bands.

Acknowledgements The authors at Columbia University acknowledge support from the Nanoscale Science and Engineering Initiative of the National Science Foundation under grant numbers ECS-05-07111 and CHE-0117752. The authors at LPA and LPQM acknowledge support from the GDRI "Graphene-Nanotubes".

References

[1] Z. Liu, S. Tabakman, K. Welsher, and H. Dai, Nano Res. **2**, 85–120 (2009). 10.1007/s12274-009-9009-8.
[2] J. S. Lauret, C. Voisin, G. Cassabois, J. Tignon, C. Delalande, P. Roussignol, O. Jost, and L. Capes, Appl. Phys. Lett. **85**(16), 3572–3574 (2004).
[3] P. Avouris, Z. Chen, and V. Perebeinos, Nature Nanotechnol. **2**(10), 605–615 (2007).
[4] R. Saito, G. Dresselhaus, and M. S. Dresselhaus, Physical Properties of Carbon Nanotubes (Imperial College Press, London, 1998).
[5] M. Y. Sfeir, T. Beetz, F. Wang, L. Huang, X. M. H. Huang, M. Huang, J. Hone, S. O'Brien, J. A. Misewich, T. F. Heinz, L. Wu, Y. Zhu, and L. E. Brus, Science **312**(5773), 554–556 (2006).

[6] S. Reich, C. Thomsen, and J. Maultzsch, Carbon Nanotubes: Basic Concepts and Physical Properties (Wiley-VCH, Weinheim, 2004).
[7] E. B. Barros, A. Jorio, G. G. Samsonidze, R. B. Capaz, A. G. S. Filho, J. M. Filho, G. Dresselhaus, and M. S. Dresselhaus, Phys. Rep. **431**(6), 261–302 (2006).
[8] M. S. Dresselhaus, G. Dresselhaus, R. Saito, and A. Jorio, Annu. Rev. Phys. Chem. **58**(1), 719–747 (2007).
[9] J. S. Lauret, C. Voisin, G. Cassabois, C. Delalande, P. Roussignol, O. Jost, and L. Capes, Phys. Rev. Lett. **90**(5), 057404 (2003).
[10] J. S. Lauret, C. Voisin, S. Berger, G. Cassabois, C. Delalande, P. Roussignol, L. Goux-Capes, and A. Filoramo, Phys. Rev. B **72**(11), 113413 (2005).
[11] M. J. O'Connell, S. M. Bachilo, C. B. Huffman, V. C. Moore, M. S. Strano, E. H. Haroz, K. L. Rialon, P. J. Boul, W. H. Noon, C. Kittrell, J. Ma, R. H. Hauge, R. B. Weisman, and R. E. Smalley, Science **297**(5581), 593–596 (2002).
[12] S. Berger, C. Voisin, G. Cassabois, C. Delalande, P. Roussignol, and X. Marie, Nano Lett. **7**(2), 398–402 (2007).
[13] S. Berciaud, L. Cognet, and B. Lounis, Phys. Rev. Lett. **101**(7), 077402 (2008).
[14] R. Matsunaga, Y. Miyauchi, K. Matsuda, and Y. Kanemitsu, Phys. Rev. B **80**(11), 115436 (2009).
[15] S. Tretiak, Nano Lett. **7**(8), 2201–2206 (2007).
[16] H. Zhao and S. Mazumdar, Phys. Rev. Lett. **93**(15), 157402 (2004).
[17] V. Perebeinos, J. Tersoff, and P. Avouris, Nano Lett. **5**(12), 2495–2499 (2005).
[18] I. B. Mortimer and R. J. Nicholas, Phys. Rev. Lett. **98**(2), 027404 (2007).
[19] A. Srivastava, H. Htoon, V. I. Klimov, and J. Kono, Phys. Rev. Lett. **101**(8), 087402 (2008).
[20] R. Matsunaga, K. Matsuda, and Y. Kanemitsu, Phys. Rev. Lett. **101**(14), 147404 (2008).
[21] J. Maultzsch, R. Pomraenke, S. Reich, E. Chang, D. Prezzi, A. Ruini, E. Molinari, M. S. Strano, C. Thomsen, and C. Lienau, Phys. Rev. B **72**(24), 241402 (2005).
[22] F. Wang, G. Dukovic, L. E. Brus, and T. F. Heinz, Science **308**(5723), 838–841 (2005).
[23] V. Perebeinos, J. Tersoff, and P. Avouris, Phys. Rev. Lett. **94**(2), 027402 (2005).
[24] F. Plentz, H. B. Ribeiro, A. Jorio, M. S. Strano, and M. A. Pimenta, Phys. Rev. Lett. **95**(24), 247401 (2005).
[25] Y. Miyauchi and S. Maruyama, Phys. Rev. B **74**(3), 035415 (2006).
[26] Y. Murakami, B. Lu, S. Kazaoui, N. Minami, T. Okubo, and S. Maruyama, Phys. Rev. B **79**(19), 195407 (2009).
[27] S. Berciaud, L. Cognet, P. Poulin, R. B. Weisman, and B. Lounis, Nano Lett. **7**(5), 1203–1207 (2007).
[28] O. N. Torrens, M. Zheng, and J. M. Kikkawa, Phys. Rev. Lett. **101**(15), 157401 (2008).
[29] P. M. Vora, X. Tu, E. J. Mele, M. Zheng, and J. M. Kikkawa, Phys. Rev. B **81**(15), 155123 (2010).
[30] J. Lefebvre and P. Finnie, Nano Lett. **8**(7), 1890–1895 (2008).
[31] P. T. Araujo, S. K. Doorn, S. Kilina, S. Tretiak, E. Einarsson, S. Maruyama, H. Chacham, M. A. Pimenta, and A. Jorio, Phys. Rev. Lett. **98**(6), 067401 (2007).
[32] T. Michel, M. Paillet, J. C. Meyer, V. N. Popov, L. Henrard, and J. L. Sauvajol, Phys. Rev. B **75**(15), 155432 (2007).
[33] C. L. Kane and E. J. Mele, Phys. Rev. Lett. **93**(19), 197402 (2004).
[34] S. Berciaud, C. Voisin, H. Yan, B. Chandra, R. Caldwell, Y. Shan, L. E. Brus, J. Hone, and T. F. Heinz, Phys. Rev. B **81**(4), 041414 (2010).
[35] M. Y. Sfeir, F. Wang, L. Huang, C. C. Chuang, J. Hone, S. P. O'Brien, T. F. Heinz, and L. E. Brus, Science **306**(5701), 1540–1543 (2004).
[36] C. Manzoni, A. Gambetta, E. Menna, M. Meneghetti, G. Lanzani, and G. Cerullo, Phys. Rev. Lett. **94**(20), 207401 (2005).
[37] C. D. Spataru, S. Ismail-Beigi, L. X. Benedict, and S. G. Louie, Phys. Rev. Lett. **92**(7), 077402 (2004).
[38] J. Deslippe, C. D. Spataru, D. Prendergast, and S. G. Louie, Nano Lett. **7**(6), 1626–1630 (2007).
[39] E. Malic, J. Maultzsch, S. Reich, and A. Knorr, Phys. Rev. B **82**(11), 115439 (2010).
[40] F. Wang, D. J. Cho, B. Kessler, J. Deslippe, P. J. Schuck, S. G. Louie, A. Zettl, T. F. Heinz, and Y. R. Shen, Phys. Rev. Lett. **99**(22), 227401 (2007).
[41] P. May, H. Telg, G. Zhong, J. Robertson, C. Thomsen, and J. Maultzsch, Phys. Rev. B **82**(19), 195412 (2010).

